Front. Phys. China (2006) 3: 305－316
DOI 10.1007/s11467-006-0029-5

REVIEW ARTICLE

LI Zhi-bing, DENG Shao-zhi, XU Ning-sheng

Mechanism of field electron emission from carbon nanotubes

Abstract Field electron emission (FE) is a quantum tunneling process in which electrons are injected from materials (usually metals) into a vacuum under the influence of an applied electric field. In order to obtain usable electron current, the conventional way is to increase the local field at the surface of an emitter. For a plane metal emitter with a typical work function of 5 eV, an applied field of over 1 000 V/μm is needed to obtain a significant current. The high working field (and/or the voltage between the electrodes) has been the bottleneck for many applications of the FE technique. Since the 1960s, enormous effort has been devoted to reduce the working macroscopic field (voltage). A widely adopted idea is to sharpen the emitters to get a large surface field enhancement. The materials of emitters should have good electronic conductivity, high melting points, good chemical inertness, and high mechanical stiffness. Carbon nanotubes (CNTs) are built with such needed properties. As a quasi-one-dimensional material, the CNT is expected to have a large surface field enhancement factor. The experiments have proved the excellent FE performance of CNTs. The turn-on field (the macroscopic field for obtaining a density of 10 $\mu A/cm^2$) of CNT based emitters can be as low as 1 V/μm. However, this turn-on field is too good to be explained by conventional theory. There are other observations, such as the non-linear Fowler-Nordheim plot and multi -peaks field emission energy distribution spectra, indicating that the field enhancement is not the only story in the FE of CNTs. Since the discovery of CNTs, people have employed more serious quantum mechanical methods, including the electronic band theory, tight-binding theory, scattering theory and density function theory, to investigate FE of CNTs. A few theoretical models have been developed at the same time. The multi-walled carbon nanotubes (MWCNTs) should be assembled with a sharp metal needle of nano-scale radius, for which the FE mechanism is more or less clear. Although MWCNTs are more common in present FE applications, the single-walled carbon nanotubes (SWCNTs) are more interesting in the theoretical point of view since the SWCNTs have unique atomic structures and electronic properties. It would be very interesting if people can predict the behavior of the well-defined SWCNTs quantitatively (for MWCNTs, this is currently impossible). The FE as a tunneling process is sensitive to the apex-vacuum potential barrier of CNTs. On the other hand, the barrier could be significantly altered by the redistribution of excessive charges in the micrometer long SWCNTs, which have only one layer of carbon atoms. Therefore, the conventional theories based upon the hypothesis of fixed potential (work function) would not be valid in this quasi-one-dimensional system. In this review, we shall focus on the mechanism that would be responsible for the superior field emission characteristics of CNTs. We shall introduce a multi-scale simulation algorithm that deals with the entire carbon nanotube as well as the substrate as a whole. The simulation for (5, 5) capped SWCNTs with lengths in the order of micrometers is given as an example. The results show that the field dependence of the apex-vacuum electron potential barrier of a long carbon nanotube is a more pronounced effect, besides the local field enhancement phenomenon.

Keywords carbon nanotube, field emission, multi-scale simulation

PACS numbers 68.37.Vj , 61.46.Fg, 71.15.Pd

LI Zhi-bing (✉), DENG Shao-zhi, XU Ning-sheng
State Key Laboratory of Optoelectronic Materials and Technologies, School of Physics and Engineering, Sun Yat-Sen University, Guangzhou 510275, China
E-mail: stslzb@zsu.edu.cn

Received June 16, 2006

1 Introduction

The electron source based on field electron emission (FE) has several attractive advantages, in contrast to the conventional electron source of hot cathodes. An obvious advantage is

that the FE need not heat the electron up to a high temperature as in the case of hot cathodes, thus saving much energy in principle. The FE technique can be combined with the microelectronic integrated technique and would finally become portable. The applications of FE include flat panel displays, high-power vacuum electronic devices, microwave-generation devices, and vacuum microelectronic devices.

Serious investigations took off in the late 1960s and early 1970s, when Spindt-type cathodes were developed. These are basically micro-fabricated molybdenum tips in gated configuration [1, 2]. Subsequently, silicon microtip arrays were fabricated, and silicon vacuum micro-triodes were introduced. This development led to the creation of a new area of research called "vacuum microelectronics". The Mo microtip arrays and Si microtip arrays were subsequently developed for large-area addressable electron emitters for prototype field emission displays. High-resolution displays based on this novel technology were being produced by various commercial organizations and demonstrated since the beginning of the 1990s. Cold cathodes utilize the surface field enhancement at the apex of each nanoscale protrusion (or microtip) to lower the threshold voltage enabling FE. The field for obtaining current density of 10 $\mu A/cm^2$ is usually defined as the turn-on field. Although the macroscopic field needed for appreciable emission has been considerably reduced (the turn-on field is reduced from a few kV/μm to hundreds of V/μm) by the above mentioned micro-fabricated techniques, the working field is still too high. The high field results in ionization of the residual gases, emitter damage, and large current fluctuation. To improve the operation of FE devices, people have to seal the emitter in a high vacuum environment. It has been found that the emitters coated with inert materials such as amorphous diamond-like-carbon [3,4] have been shown to have electron emission properties and robustness much superior to Mo and Si micro/nanotip arrays. However, the fabrication facility required and the fabrication processes are relatively expensive and complicated. This is still the prime obstacle that hinders FE from becoming a popular household electron source such as for television displays and light elements.

Since Iijima first reported the discovery of carbon nanotubes (CNTs) in a simple arc-evaporation apparatus [5] in 1991, the unique physical properties of CNTs have attracted great interest from both academic studies and industrial applications [6,7,8]. The high aspect ratio of CNTs is the main feature that attracts people since it would imply an extremely large field enhancement at the apexes of CNTs. This provides a great opportunity for using such a material to obtain electron emission at rather low fields. It has been reported that CNTs may emit electrons with driving voltages comparable to that of a solid-state device [9]. The CNTs also have good electrical conductivity, high melting points, good chemical inertness, and high mechanical stiffness. All these are welcome properties for FE. With such exciting opportunities, there is now a flurry of activities in theoretical investigations and experimental explorations. In 1995, the FE of nanotubes from an isolated single MWCNT was first reported by Rinzler *et al*. [10] and FE from a MWCNT film was reported by de Heer *et al*. [11]. Subsequently, many experimental studies on FE from MWCNTs [12,13,14,15] and SWCNTs [14,16,17] were reported. Experimental observations of individual CNT have been accumulating [18, 19, 20, 21, 22]. Significant emission can be observed in a macroscopic field much lower than the normal emitters. In CNT films, Ma *et al*. recorded the turn-on field for obtaining an emission current density of 10 $\mu A/cm^2$ to be ~2.1 V/μm and the threshold field for obtaining a current density of 10 mA/cm^2 to be ~3.0 V/μm [23]. The turn-on field can be even as low as 1 V/μm [24,25]. Another advantage is that the energy spread is far narrower than for thermoelectronic sources. The width of the energy distribution (full width at half maximum, or FWHM) can be as low as 0.11 eV, but typical values are around the 0.2 eV [20,26,27]. Large area FE based on CNTs have become possible after two major achievements including: (i) the capability of aligning carbon nanotubes vertically to the substrate surface [28] and (ii) the success in growing carbon nanotube towers in array form [29]. The field electron emission based on CNT materials has found applications in flat panel displays [30,31], light elements [32,33], sensor devices [34,35,36,37], and miniature high-brightness electron sources for both electron microscope [38] and parallel e-beam lithography systems [39]. A new generation of electron source based on this technique has become foreseeable.

The set up of the CNT-based field electron emission system is schematically illustrated in Fig. 1. The CNT is mounted on the metal substrate (tungsten for instance) vertically. When a voltage is applied between the cathode and the anode, electrons are driven to the tip of the CNT and have a certain probability to tunnel through the apex-vacuum barrier by quantum mechanics. The central theoretical issue has been the mechanism underlying the field emission from CNTs observed at an applied field as low as 1 V/μm. To explain such a finding by the classical Fowler-Nordheim (FN) theory [40,41], some researchers have reported a field enhancement factor as large as several thousands, which is too large for a realistic CNT emitter. More serious investigation is required.

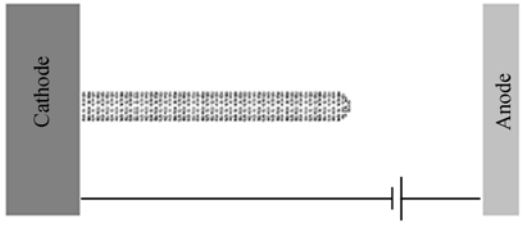

Fig. 1 Setup for field emission from a SWCNT. The SWCNT is vertically mounted on the tungsten substrate. The distance between the cathode and anode is unphysical.

The electronic bands of SWCNTs of various atomic structures were obtained within the first two years just after

the discovery of CNTs [42, 43, 44, 45, 46]. It is known that the conductivity of a SWCNT depends on the diameter and the atomic structure. The SWCNT can either be metallic or semiconducting. The field emission properties have been calculated by the tight-binding theory and scattering theory [47, 48, 49]. In recent years, quantum mechanical simulations of the field emission of CNTs have been performed [50, 51,52,53,54,55]. Density-functional theory (DFT) has been employed to calculate the electrostatic fields, charge distributions and electronic states near the tips [51, 52, 56, 57]. The earlier works were limited by the computational efficiency and capacity available. In such calculations, the fields at the tip are often set to a very high value following the field enhancement factor predicted by the classical theory [54,55]. The validity of this assumption is not easy to examine since it is difficult to determine the surface field, thus the field enhancement factor in experiments. On the other hand, extra charges have been found to have significant effects on the potential at the tip and subsequently on the emission process [53]. However, the exact amount of extra charges around the tip is not easy to determine in the simulations [53]. Zheng *et al*. [55] have developed a procedure to simulate the charge distributions and electrostatic fields along a 1-μm long capped (5,5) SWCNT under the applied fields of 10—14 V/μm and a realistic experimental setup. This and a more detailed simulation [58] enabled one to calculate the field enhancement factor through the simulated potential barrier. It revealed a new mechanism besides the well-known field enhancement. That is the field dependence of the apex-vacuum electron potential barrier. The effective work function at the apex where the electrons are to be emitted is reduced by the applied field significantly, which leads to the low voltage FE of CNTs. There are other hints for the invalidity of classical FN theory. For instance, the linear FN plot predicted by the classical FN theory is found to be disregarded in some experiments [15,59,60,61,62,63]. Both single-peak and multi-peaks have been observed in the field emission energy distribution spectra [20, 64, 65, 66], which would be related to the special features of CNTs and have great theoretical interests.

The article will be arranged as follows. In Section 2, some basic facts of CNTs will be introduced. In Section 3, after a brief review of the conventional Forlor-Nordheim theory, we will discuss several mechanisms that would be responsible for field electron emission of CNTs. The main ideas of the multi-scale algorithm for simulations of entire CNTs are outlined in Section 4. The simultion of the (5, 5) SWCNT with capped end will be shown as an example in Section 5. Section 6 is devoted for discussions and conclusions.

2 The structure and electronic bands of CNTs

The CNTs produced in the earlier days usually contain several walls. Each wall is a rolled-up graphene layer in which each atom is bound to three neighbors in a honeycomb-like structure [Fig. 2 (a)], and ranged in outer diameter from about 3 nm to 30 nm. In 1993, single-walled CNTs (SWCNTs) were synthesized [67,68]. The SWCNTs have very small diameters, typically 1 nm or even smaller.

The structure of an individual SWCNT is specified by a vector ($\boldsymbol{C}$) joining two equivalent points on the planar graphene lattice. By use of the unit cell base vectors of the graphene lattice, $\boldsymbol{a}_1$ and $\boldsymbol{a}_2$, the vector can be expressed as $\boldsymbol{C} = n\,\boldsymbol{a}_1 + m\,\boldsymbol{a}_2$. Then each integer pair (n, m) with $n > m$ represents a possible tube structure [Fig. 2 (b)]. The lattice constant $a = |\boldsymbol{a}_1| = |\boldsymbol{a}_2| = 0.246$ nm. The magnitude of $\boldsymbol{C}$ is $|\boldsymbol{C}| = a\sqrt{(n^2 + nm + m^2)}$, and the diameter of the tube is $d_t = |\boldsymbol{C}|/\pi$. The SWCNTs are usually divided into three species according to their atomic structures. They are the armchair carbon nanotubes of $n = m$ [Fig. 2 (c)], the zigzag carbon nanotubes of $m = 0$ [Fig. 2 (d)], and the chiral carbon nanotubes if neither $n = m$ nor $m = 0$ [Fig. 2 (e)]. Detailed discussions about the structures can be found in Refs. [42,69]. A SWCNT (infinite long) can be either metallic or semiconducting, depending on how the graphene sheet is rolled up into the tube [42,43,44, 45, 46,69,70]. It has been known that metallic conduction occurs when $n - m = 3q$, where q is an integer or zero.

The band structure of SWCNTs can be obtained from the well-known band structure of graphene, if one neglects the small distortion due to the curvature of SWCNTs. The electron energy of graphene at a point of the Brillouin zone specified by the wave vector (k_x, k_y) has the expression [71],

$$E_{2\mathrm{D}}(k_x, k_y) = \pm\gamma_0 \left\{1 + 4\cos\left(\frac{\sqrt{3}k_x a}{2}\right)\cos\left(\frac{k_y a}{2}\right) + 4\cos^2\left(\frac{k_y a}{2}\right)\right\}^{1/2} \quad (1)$$

where $\gamma_0 = 2.7$ eV is the nearest-neighbor transfer integral. The minus (plus) sign is for the bonding (antibonding) σ and π(σ^* and π^*) bands. The Fermi level is at the point where the π level and the π^* level are degenerate. Since the circumferences of carbon nanotubes are in atomic dimensions, the motion in the circumferential direction is confined hence its energy is discretized. Denote the wave number in the direction of the tube axis as k, the wave vector can be written as

$$k_x = \frac{a(m-n)}{2L}k + \frac{\sqrt{3}\pi a}{L^2}(n+m)\nu \quad (2)$$

$$k_y = \frac{\sqrt{3}a(m+n)}{2L}k + \frac{\pi a}{L^2}(n-m)\nu \quad (3)$$

where ν is an integer. For instance, $k_y = k$ of the (n,n) armchair is in the direction of the tube axis; in the circumferential direction,

$$k_x = \frac{\nu}{n}\frac{2\pi}{\sqrt{3}a}, \quad \nu = 1, \cdots, n \quad (4)$$

The energy dispersion relations for armchair SWCNTs are obtained by substituting Eq. (4) into Eq. (1). The Fermi level is at $\nu = 5$ and $k_y = k = \frac{2\pi}{3a}$. The linear density of states in the vicinity of the Fermi level is a constant, N_f =

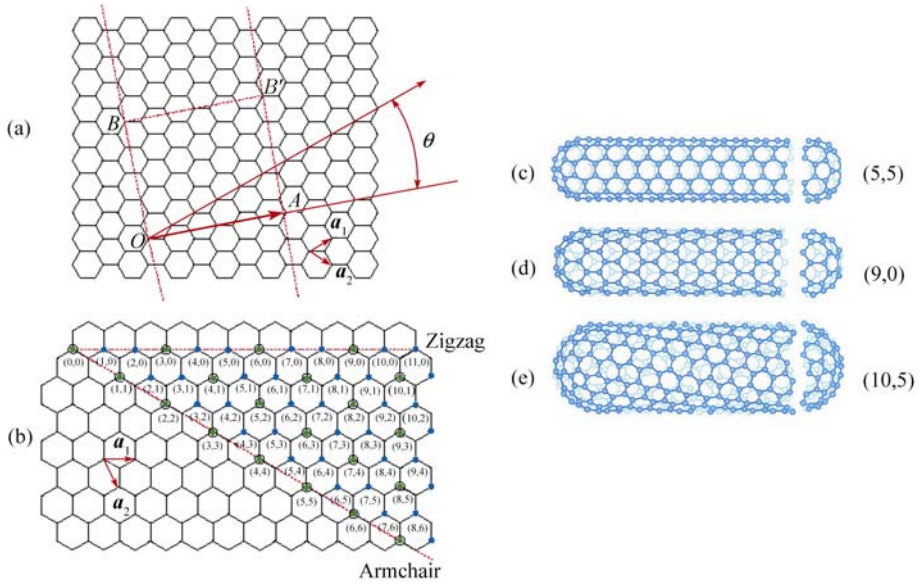

Fig. 2 The structures of single-walled carbon nanotubes. (**a**) The lattice of a graphene sheet; $\boldsymbol{a}_1$ and $\boldsymbol{a}_2$ are two unit vectors of the lattice; the sheet is to be wrapped by coinciding O and A (B and B'). (**b**) The labels of sites. (**c**) The armchair SWCNT. (**d**) The zigzag SWCNT. (**e**) The chiral SWCNT.

$8/\sqrt{3}\pi a\gamma_0$.

The band structures for MWCNTs have not been conclusive. Saito and colleagues calculated the band structure of double-walled nanotubes using the tight-binding method [72]. They showed that the interlayer coupling had little effect on the electronic properties of the individual tubes. However Charlier and his colleagues found that the coupling between layers would change the metallic tube to semiconducting tube in some circumstances [73,74].

Table 1 Typical electronic properties of CNTs and graphite concerned with field emission.

parameters	CNT	Graphite	Reference
Resistivity /(Ω.cm)	~(5.1－5.8)×10^{-6}	1.375×10^{3}	[75]
Conductance /(kΩ)$^{-1}$	$2e^2/h$		[76]
Work function /eV	~4.6－4.8	5.0	[77]

A physical property that has a strong effect on FE is the work function of CNTs and a number of studies were carried out to determine this [77,78,79]. In an investigation using in situ transmission electron microscopy by Gao *et al*. [77], the majority of the MWNTs were found to have values of work function in the range of 4.6－4.8 eV at the tips, which is ~0.2－0.4 eV lower than that of a bulk carbon sample, while a small fraction of them have a work function of ~5.6 eV, which is about 0.6 eV larger than that of the carbon. Also, for MWNTs of diameters within the range of 14－55 nm, the tip work function is essentially not affected by their diameter.

3 The mechanisms

In the past ten years, many calculations and simulations have been devoted to understand the mechanism of FE from CNTs and the related problems. As CNTs have many possible structures, of which the conductivity and density of states are different, there would be several mechanisms playing roles together or separately for different structures. The common features of CNTs used in FE shall be the high apex ratio and the $\pi(\pi^*)$ bonding (antibonding) orbitals for valence (conducting) electrons. The multi-walled CNTs having larger radii would resemble a metal wire. The single-walled CNTs having small radii would be more complicated since they can be either metallic or semiconducting. The detailed structure of the apex, e.g., open-ended or cap-ended, and how the dangling bonds of carbon are saturated, would all have important effects on the FE. In the present article, we do not attempt to give a complete review in any sense to the existing literatures on this topic. Only a few theories that are either widely accepted or reflecting the common features of the CNTs will be discussed.

3.1 The Fowler-Nordheim theory

The Fowler-Nordheim (FN) theory dates back to 1928 and is the standard theory for FE from metallic planes. In the classical FN theory, the potential barrier on the metal surface is presumably a combination of the ramp potential and the image potential of the emission electron. The ramp potential is associated to a surface field, denoted by E. The barrier potential is then written as

$$U(z) = E_{\mathrm{F}} + \phi - ezE - \frac{e^2}{16\pi\varepsilon_0 z} \tag{5}$$

where ϕ is the work function of the metal; E_{F} is the Fermi level of the metal; z is the normal coordinate of the metal

surface. It is valid for $z > z_0$, with z_0 defined by $U(z_0) = E_F$. The transmission probability is calculated by the JWKB approximation. Following Forbes's parameterization [80], the emission current of a FN-type theory for general-barrier can be written as

$$I = \lambda a\phi^{-1}E^2 \exp\left(-\mu b\phi^{3/2}/E\right) \tag{6}$$

where a and b are known constants, μ and λ are "generalized correction factors" that do not or only weakly depend on E. The surface field is usually larger than the applied field E_{appl}. The field enhancement factor is defined as $\gamma = E/E_{appl}$ Therefore, the plot of $\ln\left(I/E_{appl}^2\right)$ versus $1/E_{appl}$ is a straight line, with a slope $-\mu b\phi^{3/2}/\gamma$. This plot is the famous FN plot. The straight FN plot has been known as the best model of FE experiments. Provided μ, one can extract γ from the slope of an FN plot. The field enhancement factor obtained in this way will be referred to as the phenomenological field enhancement factor (γ_{phe}) [58]. A recent comprehensive discussion on the validity and the experimental implications of the FN theory has been given by Forbes [80,81].

The experimental observations of CNT field electron emission do not always give straight FN plots [15,59,60,61, 62,63]. There have been many explanations. For instance, it has been attributed to the curvature of the apex [82]; to small size and strong local fields that lead to localized states at the apex [20,59,83]; to the space charge vs thermionic emission [15,60]; to the adsorbate effects [21]; to the back contact resistance [84]; and so on. The emission current from CNTs have been estimated by taking into account the band structures of CNTs [47,48,49]. It is found that current depends on the chirality only at very high temperatures [49]. The method of transfer-matrix and Green's functions should be a more reliable method for calculation of emission current [85, 86]. However, this method has been quite tedious. The shape of the energy distribution strongly suggests that the electrons are not emitted from a metallic continuum, but from energy bands of 0.2—0.4 eV width [20]. Assuming that most emitting electrons come from the π^* orbitals of the first layer (on the side of the anode) and have the Fermi energy (approximately), the emission current can be simply estimated as

$$I = \nu q_\pi D(E_F) \tag{7}$$

where q_π is the charge of electrons in the π^* orbitals of the first layer, and ν is the collision frequency that can be estimated from the average kinetic energy of π^* electrons as $\nu = E_k(\pi^*)/h$ or other methods [58]. The order of ν should be 10^{14}Hz. The transmission coefficient in the JWKB approximation is

$$D(E_F) = \exp\left(-\frac{2}{\hbar}\mathrm{Im}\int\sqrt{2m[E_F - U(z)]}\,\mathrm{d}z\right) \tag{8}$$

All methods for the estimation of emission current mentioned above are based on the apex-vacuum potential barrier $U(z)$, which defines the main trend of FE characteristic. In the following text, we shall focus on the calculation of $U(z)$.

3.2 The field enhancement mechanism

The apex-vacuum potential barrier is roughly represented by the surface field enhancement factor defined as the ratio of the surface field and the applied macroscopic field. A common but not yet verified view is that the high aspect ratio of a CNT leads to the low turn-on macroscopic field because the intense electric field concentration at the apex surface reduces the apex-vacuum potential barrier (AVPB). This mechanism will be referred to as field enhancement mechanism (FEM). According to classical electrostatics, the field enhancement factor γ is approximately equal to the length/radius aspect ratio [87]. For more than half a century, engineers have made great effort to purchase metallic apexes (apex arrays) of high aspect ratio. Since the CNTs have extremely high aspect ratio, it is natural to expect them to have large γ and to have great possibility to be good FE emitters. In fact it is the first motivation for this application of CNTs.

A classical model for a CNT emitter is the metallic hemisphere supported on a shank (Fig. 3). Instructive comments on the classical field enhancement factor (γ_{cl}) have been made by Forbes, Edgcombe, and Valdrè [87]. In a good approximation, γ_{cl} is given by

$$\gamma_{cl} = 2.5 + \frac{L}{\rho} \tag{9}$$

where ρ is the radius of the apex half-sphere and L is the distance of the center of the half-sphere to the substrate surface.

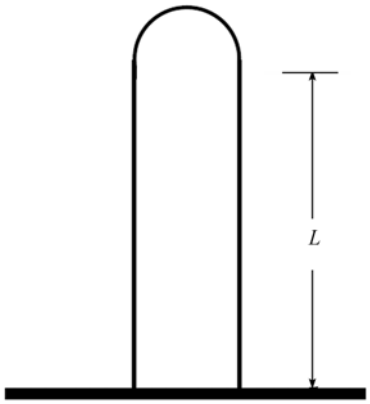

Fig. 3 The hemisphere supported on a shank.

Kokkorakis, Modinos, and Xanthakis (KMX) proposed a model that the CNT was simulated by a cylindrical array of touching spheres, each sphere representing an atom of the tube [88]. For the capped SWCNT, they obtained

$$\gamma_{cl} = 5.93 + 0.73(L/\rho) - 0.0001(L/\rho)^2 \tag{10}$$

It is consistent with the finite element calculations of Edgcombe and Valdrè for $100 < L/\rho < 500$ [89]. To the open CNTs, the KMX model suggests that the field enhancement factor is determined primarily by the thickness of the wall and not by the radius of the tube. Taking into account the carbon polarization, Adessi and Devel calculated the field enhancement factor by means of a self-consistent resolution of Possion's equation [90]. Their numerical results show a logarithmic saturation of field enhancement against the CNT length. It has been noticed that the local fields at the apex of CNTs may depend on the angles to the axis of the CNT [82].

Comparing the theoretical field enhancement factor with the experiments is not straightforward, anyhow. Conventionally, one extracts the field enhancement factor (γ_{phe}) from the experimental slope of the FN plot (see 3.1). Since the standard F-N theory is derived for the emitters that should be considered as a metal plate, it could not be related to the real field enhancement factor defined by the ratio of the surface field and the applied field. It is also not necessarily equal to the theoretical value γ_{cl} for CNTs. In fact it has been quite confusing in experimental values of the field enhancement factor [21, 91, 92]. The values of γ_{phe} from several hundreds to several thousands have been reported.

The FEM would not be valid for CNTs of small diameters, especially for SWCNTs. Assuming that CNTs have a work function of 5.eV as graphene, the surface field must be in the order of several Volts per nm in any case for that significant field emission to be observed. If the low turn-on macroscopic field were due to the FEM, one would need a field enhancement factor as large as several thousands for CNTs. Although this would be consistent with the electrostatics conclusion that the field enhancement factor for a long metal rod is approximately the same as its aspect ratio, some problems remain unclear: (1) Can the CNTs shield the electrostatic field completely as a metal rod? If not, the field enhancement would depend on the structural properties of the CNT in a complicated way; (2) According to the classical theory, the CNTs in applied fields would become unstable as the tube length exceeds a certain value when the field strength at the tip is comparable to the atomic field due to the huge field enhancement. Since a stable FE from CNTs of micrometer scale has been observed in experiments, the classical theory must not be fully correct for long CNTs; (3) Is there any unknown quantum effect thatp lays a role in the nanoscale tube tip? It has been found that FE is closely related to the local electronic states in the tip [20,59,83]; and (4) In the classical FN theory, the potential barrier between a metal and the vacuum is a combination of the ramp potential of the applied field and theimage potential of the emission electron. The latter arisesfrom a macroscopic mean effect and is found field-independent. As the apex of the CNT is in nanoscale, the conceptof image potential would no longer be applicable.

To clarify these issues, we need to know the detailed electronic structure of the CNTs under applied external fields, especially the charge distribution and the electron potential in the tip region. A quantum mechanical investigation is thus necessary. However, since a carbon nanotube is a huge molecule that consists of hundreds of thousands to millions of carbon atoms, an atomic level calculation of the entire tube is still far from achievable. Most of the previous calculations based on DFT [51,52,56,57] were carried out on nanotubes whose lengths are only a few nanometers because of the limitation of computational resources. To compare with experimental results, a factor $L_{\mathrm{tube}}/L_{\mathrm{tip}}$ is introduced to scale the external field in the simulation on a short SWCNT [50], where L_{tube} represents the length of the tube of experimental usage while L_{tip} is the length adopted in the calculation. Based on this simplified model, some suggestive results have been obtained. Since L_{tip} is on the order of a few nanometers while L_{tube} is usually a few μm, the scaled field E_{scal} is much stronger than the applied field E_{appl}. The relationship between the scaled field and the localized electronic states at the tip is still not clear, and the amount of excessive charges around the tip has not been determined in previous calculations.

3.3 The apex structure mechanism

Since the CNT apex consists of a small number of atoms, the emission current will be greatly affected by the apex structure and adsorbates [21,22]. The defects or decorated atoms at the apex could play as electron donors or acceptors, and create localized states. The resonant energy levels would be formed around the defects and adsorbates that the tunneling probability of some channels would be increased dramatically. The energy distribution analysis of the emission shows that the density of states at the tip is non-metallic, appearing in the form of localized states with well-defined energy levels [20]. The electron transfer between the adsorbates and the CNT body forms an electric dipole (and/or quadrupoles) at the apex and changes the local field. The FE assisted by special apex structure will be referred to as the apex structure mechanism (ASM). It has been observed that the hydrogenation of the tube wall transforms a metallic CNT into a semiconducting one [93], that O_2 exposure increases the turn-on field of SWCNTs and decreases the FE efficiency [94], and that the adsorption of H_2O enhances the field emission current. However, experimental observations have not been conclusive so far [63,93,94,95].

To understand the dependence of FE upon the atomic structures of CNT apexes, careful simulations via the DFT have been done [96－102]. There are contradictory conclusions about the effect of adsorbates. Zhou *et al*. [51] and Kim *et al*. [95, 103] obtained the local density of states (LDOS) at the apex by ab initio methods. They found that the LDOS at the charge-neutrality level was suppressed by the hydrogen. They therefore concluded that hydrogen adsorption reduces FE current density. By contrast, Mayer *et al*. calculated the AVPB using a dipole and point charge model [104]. They assumed that the surface barrier was re-

duced by the presence of the hydrogen, and concluded that hydrogen adsorption enhanced the FE current density. Mayer recently improved the model and illustrated the electrostatic potential around the carbon nanotube [105].

More extensive studies on this topic would obviously be useful.

3.4 The electron accumulation mechanism

Only recently, it has become possible to tackle the realistic size of SWCNTs in FE conditions by a multi-scale method involving quantum mechanics and molecular mechanics [55]. The field enhancement factor is found to be much smaller than what people expected from the classical metal wire model. The recent simulations have confirmed that the charge accumulation in both the apex and the body of CNTs leads to lowering of effective local work function (ELWF) [58], which has a more pronounced effect on FE. The lowering of ELWF due to electron accumulation is the third mechanism that we will discuss in detail in this paper. We will call this mechanism as the electron accumulation mechanism or EAM.

Through this paper, we have assumed that the SWCNT is in equilibrium with the substrate, i.e., the so-called quasi-equilibrium assumption. In the equilibrium, the Fermi level is a constant over the entire CNT and is equal to the Fermi level of the substrate. John Cumings *et al*. [106] observed that the electric field distribution varies by less than 2.5 % while the emission current has a fluctuation of 80 %. That implies that the current has less effect on the barrier and electron distribution at the tip. The equilibrium is a good approximation at least when the emission current is not too big. For the same reason, we will ignore the image effect of emission electron.

An applied field E_{appl} will drive electrons to the tip of the SWCNT. The re-distribution of electrons has two consequences. The first is that the field is shielded in the body of SWCNT, more or less, that leads to the field enhancement at the tip. However, since the SWCNT has only one layer of atoms, the shielding is not complete. There is field penetration in the tip region, so the field enhancement is smaller than the classical theory for a metal rod. Secondly, there are excessive charges accumulating along the tube, especially on the tip. In the quasi-equilibrium assumption, the charge accumulation is only possible if the neutrality level (i.e., the energy level of the neutral CNT) bends down. This happens because the applied field lowers the energies of local orbitals. The orbital with energy between the Fermi level (that is assumed to be fixed by the substrate) and the neutrality level can accommodate electrons and contribute excessive charges. A schematic picture is given in Fig. 4. When electrons fill the A zone, the SWCNT is neutral. Each electron in the orbital in the B zone contributes a charge $-e$, that forms the induced charge. The curve separating the A zone and the B zone is the neutrality level E_f^*. The barrier between the apex and the vacuum is marked by C. ϕ is the work function of the substrate, and χ is the barrier high respective to the local neutrality level at the apex.

The bending of neutrality level leads to the lowering of the apex-vacuum barrier, denoted by $\Delta\phi$. Since the electrons of the highest energy occupy the orbital of the energy of the substrate Fermi level, they see a barrier that is much lower than the affinity of an isolated neutral SWCNT. The barrier lowering corresponding to the charge accumulation at the tip is the new mechanism that favors FE besides the well-known field enhancement effect (see section 3.2). For a neutral armchair SWCNT, it is believed that the molecular orbitals below the neutrality Fermi level are π orbitals and those above are π^*. In the applied field, as mentioned above, some π^* orbitals will sink below the Fermi level. Electrons in these orbitals provide the excessive charges. Therefore the emitted electrons most probably come from the π^* orbitals near the Fermi level.

To verify the above mechanism, one should simulate the entire SWCNT. This was achieved recently by a multi-scale algorithm [55]. In the next section, we will introduce this

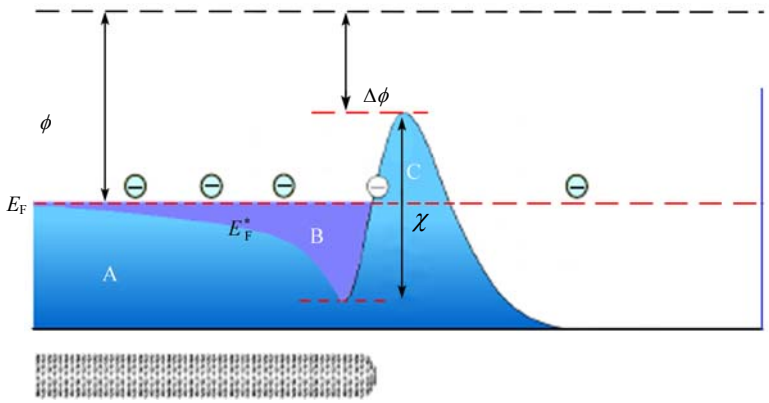

Fig. 4 A zone: filled with atom electrons; B zone: filled with induced electrons; C zone: the barrier between the apex and the vacuum. E^*_{F} is the neutrality level at the tip, $\Delta\phi$ is the barrier lowering.

method briefly.

4 The multi-scale simulation algorithm

As far as the FE is concerned, the SWCNT is a typical multi-scale system where the emission current is strongly correlated to both the mesoscopic length scale and the atomic scale at the apex. The concept of multi-scale coupling is important to understand the properties of a huge system, which are sensitive to different scales of the system. The electron emission assisted by an electric field is a tunneling process that is sensitive to the apex electronic structure, and thus needs to be treated by quantum mechanics. In experiments, the length of the SWCNT is usually in micrometers, therefore huge numbers of freedom should be considered. For instance, the (5, 5) type SWCNT of one micrometer long consists about 10^5 carbon atoms. It is still impossible to deal with the entire system using the first principle methods. Limited by the computational efficiencies and resources, all ab initio studies so far only can simulate the local properties involving hundreds of carbon atoms. The electronic properties are sensitive to both the detailed atomic arrangement (i.e., the location of defects and adsorbates) and the electronic states that would extend over the whole tube. It is a challenge for computational algorithms.

Reference [55] has proposed a multi-scale algorithm for simulation of the entire tube. It is a hybrid quantum mechanics and molecular mechanics (QM/MM) approach [107]. The entire SWCNT is firstly divided into two regions, a quantum region and a classical region (Fig. 5). In the quantum region all valence electrons and excessive electrons induced by the applied field are treated as quantum particles. The classical region covers the rest of the SWCNT in which the electrons and core ions are treated as point charges since their predominant influence on the emission is through their electrostatic potential at the tip.

The quantum region that contains 8 000 to 10 000 atoms is still too big for any ab initio method. A proper way to deal with this huge system is the linear-scaling divide-and-conquer (DAC) method [108]. It calculates the charge distribution in the quantum region by further dividing the quantum region into some subregions. Each subregion and its adjacent subregions (refer to as buffers) form a subsystem that is to be simulated by an ab initio method, as schematically shown in the enlargement on the right side of Fig. 5. The buffers are used to reduce the error of separating the subregion from the CNT. Free bonds of buffers are usually passivated by hydrogen atoms.

To estimate the excessive charge in the classical region one must take the energy band characteristic into account. For the armchair SWCNT as an example, the tight-binding theory predicts that the linear density of states (LDOS) in the vicinity of the neutrality level is a constant (see Section 2). There are also experimental evidences for the constant LDOS [109, 110]. As a consequence of the constant LDOS, in the first order of the approximation, the linear density of excessive charge (i.e., excessive charge per length) in the classical region is a linear function of the distance to the substrate, $\rho(z) = cz$, with c a constant [111]. In Ref. [55] the radial component of the electric field is ignored and ρ is written as an exponential function (Eq. (2) of Ref. [55]). For large decay constant (λ), the exponential function is consistent with the linear solution. By use of the linear ρ ansatz, one can determine the charge distribution in the classical region by one parameter, which can be fixed by the

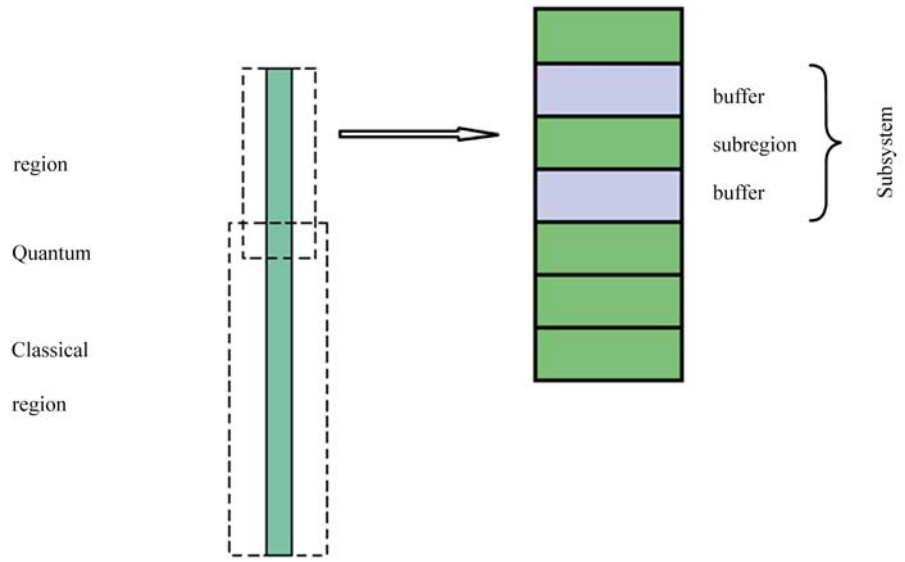

Fig. 5 The quantum region and classical region of a CNT. The quantum region is divided into subregions, each subregion and its neighbors form a subsystem.

charge density obtained by quantum simulations in the overlap region.

Since the excessive charges in the classical region have contributions to the electric field in the quantum region, one must simulate the excessive charge distribution in two regions alternatively, until self-consistency is obtained.

When the excessive charge distribution is known, it is straightforward to calculate the electrostatic potential energy [has been denoted by $U(z)$] of a point electron. It is the superposition of Coulomb potential energies created by the excess charges in the entire tube and their image charges in the substrate, and the linear decreasing energy potential generated by the applied macroscopic field.

5 The capped (5,5) SWCNT

We take the (5,5) SWCNT with the capped-end [Fig. 1(c)] as an example. The multi-scale simulation mentioned in the previous section has been applied to the capped (5, 5) SWCNT of various lengths in Refs. [55,58]. Here we will present the major results, with some new figures obtained by more precise simulation (the quantum region consists 10 000 atoms in stead of 6 000 atoms in Ref. [55,58]). The electrostatic electron potential energy in an intersection plane through the axis is given in Fig. 6. The thinnest AVEB is the path along the forward axis, therefore, forward emission is predominant. The density of excessive electrons is presented in Fig. 7. Notably, the electrons are not mostly concentrated in the first layer but in between the second and the third layers.

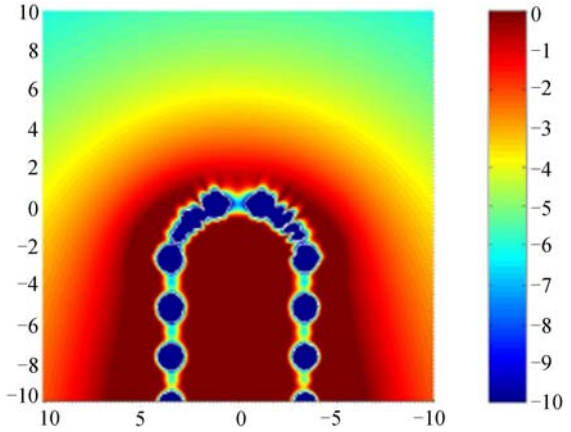

Fig. 6 The electrostatic electron potential energy (in eV) in an intersection plane through the axis of the capped SWCNT.

The change of AVEB as the applied field is shown in Fig. 8. The zero of the electron potential is the energy of vacuum in remote space out of the electric field region. The Fermi energy is at –5.08 eV. The lowering of potential height is plotted in Fig. 9. Figures 7—9 confirm the electron accumulation mechanism.

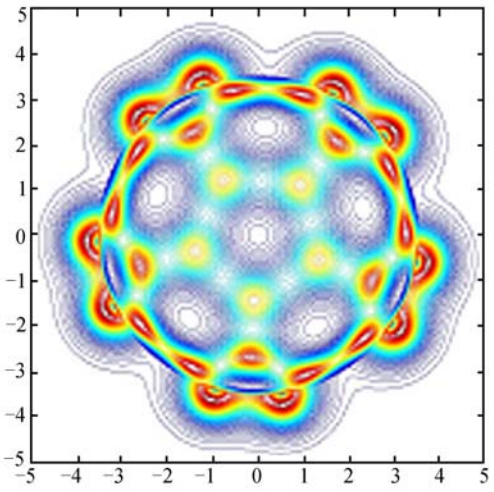

Fig. 7 The density of excessive electrons in the cap.

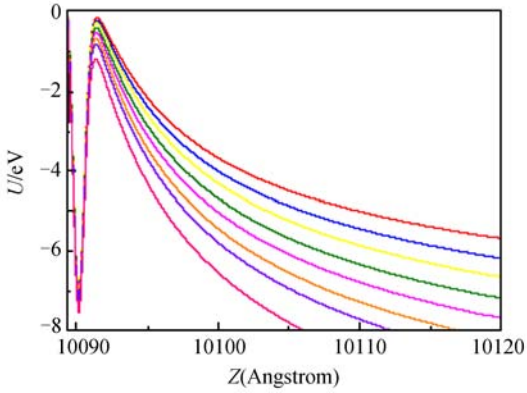

Fig. 8 Variation of electrostatic electron potential energy for the (5,5) capped SWCNT. The curves from top to bottom are corresponding to E_{appl}= 10 to 16, with step 1 V/μm, and E_{appl} =18 V/μm respectively.

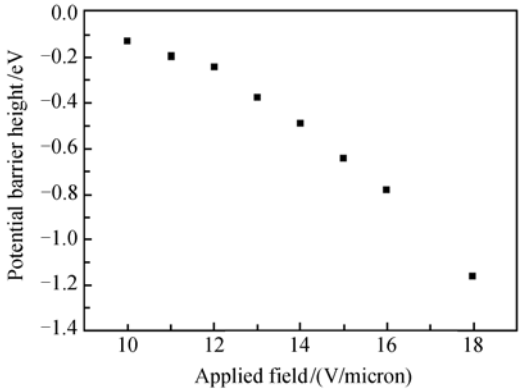

Fig. 9 The potential barrier height versus applied fields.

Define the local field E_{loc} as the highest field on the r.h.s. of the barrier. From Fig. 8, one can extract the field enancement factor $\gamma_q = E_{loc}/E_{appl}$. The subscript "q" reminds us that this field enhancement factor is obtained by quantum mechanical simulation and is different form γ_{phe} and γ_{cl} in

definition. It is found that γ_q for the one micrometer long capped (5,5) SWCNT is about 630 in contrast to the naïve estimation, 2 600, as given by the aspect ratio [recalling that the radius of the (5,5) SWCNT is 0.35 nm]. Figure 10 shows that γ_q decreases as E_{appl} increases.

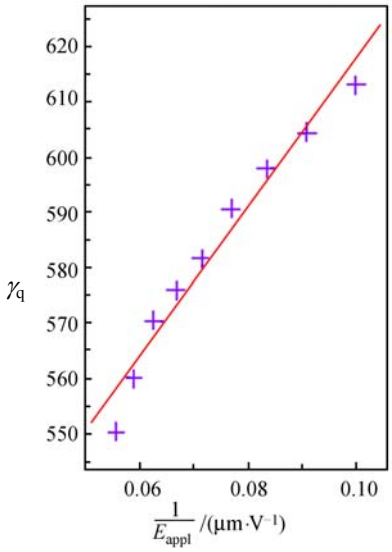

Fig. 10 The field enhancement factor of capped SWCNT. The solid curve is used to guide the eyes.

The (5, 5) capped SWCNTs of lengths from 0.5 μm to 1.1μm were simulated in Ref. [58]. The length-dependence of γ_q in the range explored can be fitted by the formula:

$$\gamma_q = \frac{E_0}{E_{appl}} + C\frac{L}{r} \tag{10}$$

where L is the length, r is the radius of the SWCNT.

Finally, the emission currents are estimated by Eqs. (7) and (8). The current as a function of the applied field is plotted in Fig. 11. The FN plot is shown as inset. Figure 12 presents the current versus the lengths.

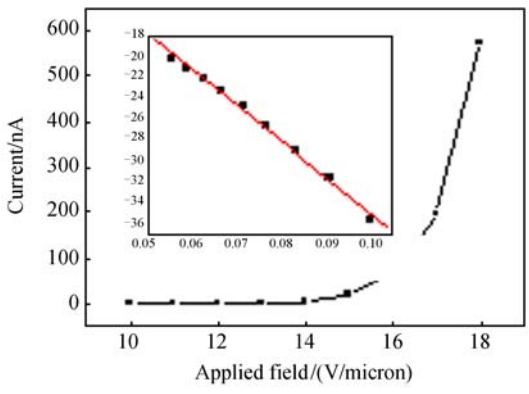

Fig. 11 The emission current as a function of the applied field. The inset is the FN plot. The lines are used to guide the eyes.

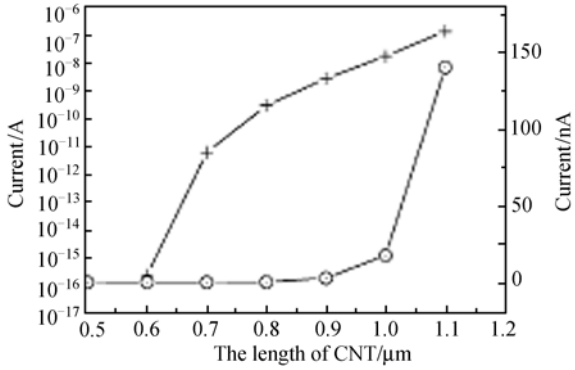

Fig. 12 The emission current as a function of lengths, at an applied field of 14 V/μm. The left vertical axis is in logarithmic scale, the right is the linear scale.

6 Conclusions and discussions

The field electron emission of carbon nanotubes has important applications. This subject is also interesting as a realistic physical system, which is well defined but non-trivial. We have addressed three mechanisms that would be responsible for the low turn-on field of CNT field electron emission. They are the field enhancement mechanism (FEM), the apex structure mechanism (ASM), and the electron accumulation mechanism (EAM).

Since the multi-scale algorithm was introduced, the mechanisms could be verified not just by experiments, but also by computer simulations. The recent progresses of multi-scale simulations have shown that the electron accumulation in the carbon nanotube has an important consequence to the effective field enhancement factor and the apex surface barrier. The effective local work function is lowered significantly following the electron accumulation and field penetration on the tip of SWCNT. This is the so-called EAM.

The present observations of both experiments and computer simulations have not excluded the other mechanisms, such as the FEM and the ASM. Since the experiments could not measure the surface field directly, the best way to examine various mechanisms should be through computational simulations. Very different from one's expectation, the field enhancement from the simulations is only in the order of a few hundreds rather than a few thousands. It is clear that the local field enhancement mechanism alone cannot account for the observed phenomenon. It must be interesting to investigate field electron emission from CNTs of different ending structures, of different chiralities, and of defects or adsorbates. In high applied fields, the quasi-equilibrium hypothesis would be violated. Also, the possibility of emitter destruction due to excessive heating needs to be thought out [112]. Further studies on these problems are requested.

In conclusions, the physical mechanism responsible for low field emission from a carbon tube would be mainly due

to the lowering of the potential barrier height and the local field enhancement due to high aspect ratio is less of a contribution. It is helpful to achieve a quantitative simulation for SWCNTs by the multi-scale algorithm. But it is still a great challenge to computational science to simulate more general structures of CNTs under more general physical conditions.

Acknowledgements The authors gratefully acknowledge financial support of the projects from the National Natural Science Foundation of China (the Distinguished Creative Group Project; Grant No. 90103028, 90306016), from the Education Ministry of China, from the Higher Education Bureau, and from the Science and Technology Commission of Guangdong Province.

References

1. Shoulders K. R., Adv. Comp., 1961, 2: 135
2. Spindt C. A., J. Appl. Phys., 1968, 39: 3504
3. Robertson J., Adv. Phys., 1986, 35: 317
4. She J. C., Xu N. S., Huq S. E., Deng S. Z., and Chen J., Appl. Phys. Lett., 2002, 81: 4257
5. Iijima S., Nature (London), 1991, 354: 56
6. de Heer W. A., Châtelain A., and Ugarte D., Science , 1995, 270: 1179
7. Baughman R. H., Zakhidov A. A., and de Heer W. A., Science, 2002, 297: 787
8. de Heer W. A. and Martel R., Phys. World, 2 000, 49: (June)
9. Xu N. S. and Hug S. E., Materials Science and Engineering, 2005, R 48: 47－189
10. Rinzler A. G., Hafner J. H., Nikolaev P., Lou L., Kim S. G., Tomanek D., Nordlander P., Colbert D. T., and Smalley R. E., Science, 1995, 269: 1550－3
11. De Heer W. A., Chatelain A., and Ugarte D., Science, 1995, 270: 1179－80
12. Collins P. G. and Zettl A., Appl. Phys. Lett., 1996, 69: 1969－70
13. Saito Y., Hamaguchi K., Hata K., Uchida K., Tasaka Y., Ikazaki F., Yumura M., Kasuya A., and Nishina Y., Nature, 1997, 389: 554－5
14. Bonard J. M., Maier F., Stoeckli T., Chatelain A., de Heer W. A., and Chatelain A., Appl. Phys. Lett. 1998, 73: 918－20
15. Xu N. S., Deng S. Z., and Chen J., Ultramicroscopy, 2003, 95: 19
16. Saito Y., Hamaguchi K., Nishino T., Hata K., Tohji K., Kasuya A., and Nishina Y., Jpn. J. Appl. Phys. 1997, 36: L1340－2
17. Liu W. M., Hou S. M., Zhang Z. X., Zhang G.M., Gu Z. N.,Ji Luo, Zhao X. Y., Xue Z. Q., Ultramicroscopy, 2003, 94: 175－182
18. Dai H., Hafner J. H., Rinzler A. G., Colbert D. T., and Smalley R. E., Nature, 1996, 384: 147
19. Fransen M. J., van Rooy Th. L., and Kruit P., Appl. Surface Science, 1999, 146: 312－327
20. Bonard J.-M., Salvetat J.-P., Stöckli T., Forró L., and Châtelain A., Appl. Phys. A, 1999, 69: 245－254
21. Dean K. A. and Chalamala B. R., Appl. Phys. Lett., 2000, 76: 375
22. Smith R. C., et al., Apple. Phys. Lett., 2005, 87: 103112
23. Ma X. C., Wang E. G., Zhou W. Z., Jefferson D. A., Chen J., Deng S. Z., Xu N. S., and Yuan J., Appl. Phys. Lett., 1999, 75: 3105
24. Murakami H., Hirakawa M., Tanaka C., and Yamakawa H., Appl. Phys. Lett., 2000, 76: 1776
25. Rao A. M., Jacques D., Haddon R. C., Zhu W., Bower C., and Jin S., Appl. Phys. Lett., 2000, 76: 3813
26. Purcell S. T., Binh V. T., and Garcia N., Appl. Phys. Lett., 1995, 67: 436
27. Fransen M. J., van Rooy Th. L., and Kruit P., Appl. Surface Science, 1999, 146: 312－327
28. Li W. Z., Xie S. S., Qian L. X., Chang B. H., Zou B. S., Zhou W. Y., Zhao R. A., and Wang G., Science, 1996, 274, 1701
29. Fan S. S., Chapline M. G., Franklin N. R., Tombler T. W., Cassell A. M. , and Dai H. Science, 1999, 283: 512
30. Talin A. A., Dean K. A., and Jaskie J. E., Solid-State Electronics, 2001, 45: 963
31. Choi W. B., Chung D. S., Kang J. H., Kim H. Y., Jin Y. W., Han I. T., Lee Y. H., Jung J. E., Lee N. S., Park G. S., and Kim J. M., Appl. Phys. Lett., 1999, 75: 3129
32. Uemura S., Yotani J., Nagasako T., Kurachi H., Yamada H., Ezaki T., Maesoba T., Nakao T., Saito Y., and Yunura M., J. SID, 2003, 11: 145
33. Chen J., Deng S. Z., and Xu, N. S., Ultramicroscopy, 2003, 95: 81
34. Collins P. G., Bradley K., Ishigami M., and Zettl A., Science, 2000, 287: 1801－1804
35. Kong J., Franklin N. R., Zhou C., Chapline M. G., Peng S., Cho K, and Dai H., Science, 2000, 287: 622－625
36. Peng S. and Cho K., Nanotechnology, 2000,11: 57－60
37. Chang H., Lee J. D., Lee S. M., and Lee Y. H., Appl. Phys. Lett., 2001, 79: 3863－3865
38. de Jonge N., Lamy Y., Schoots K., and Oosterkmp T. H., Nature (London), 2002, 420: 393
39. Semet P. V. et al., Appl. Phys. Lett., 2002, 81: 343
40. Fowler R. H. and Nordheim L., Proc. Roy. Soc. Lond. A1928, 119: 173
41. Modinos A., *Field, Thermionic, and Secondary Electron Emission Spectroscopy* (Plenum Publishing, New York, 1984)
42. Harries P. J. F., *Carbon Nanotubes and Related Structures: New Materials for the 21st Century*, Cambridge University Press 1999
43. Saito R., Fujita M., Dresselhaus G., and Dresselhaus M. S., Phys. Rev. B 1992, 46: 1804
44. Hamada N., Sawada S., and Oshiyama A., Phys. Rev. Lett., 1992, 68: 1579
45. Mintmire J. W, Dunlap B. I., and White C. T., Phys. Rev. Lett., 1992, 68: 631
46. Saito R., Dresselhaus G., Dreelhaus M. S., *Physical Properties of Carbon Nanotubes* (Imperial College Press, London, 1998)
47. Liang S. D. and N. S. Xu, Appl. Phys. Lett., 2003, 83: 1213
48. Filip V., Nicolaescu D., and Okuyama O., J. Vac. Sci. Technol. B, 2001, 19: 1016
49. Liang S. D., Huang N. Y., Deng S. Z., and Xu N. S., Appl. Phys. Lett., 2004, 85: 813
50. Luo J., Peng L. M., Xue Z. Q., and Wu J. L., Phys. Rev. B, 2002, 66: 155407
51. Han S. and Ihm J., Phys. Rev. B, 2002, 66: 241402(R)
52. Zhou G. and Kawazoe Y., Chem. Phys. Lett., 2001, 350: 386
53. Han S. and Ihm J., Phys. Rev. B, 2000, 61: 9986
54. Zhou G., Duan W. H., and Gu B. L., Phys. Rev. Lett., 2001, 87: 95504
55. Zheng X., Chen G. H., Li Z. B., Deng S. Z., and Xu N. S., Phys.

Rev. Lett., 2004, 92: 106803
56. Han S., Lee M. H., and Ihm J., Phys. Rev. B, 2002, 65: 085405
57. Buldum A. and Lu J. P., Phys. Rev. Lett., 2003, 91: 236801－1
58. Peng J., Li Z. B., He C. S., Deng X. Z., Xu N. S., Zheng X., and Chen G. H., Phys. Rev. B, 2005, 72: 235106
59. Collins P. G. and Zettl A., Phys. Rev. B, 1997, 55: 9391
60. Xu N. S., et al., Appl. Phys. Lett., 2000, 76: 2463
61. N. S. Xu, et al, Chin. Phys. Lett., 2001, 18: 1278
62. Murakami H., et al., Appl. Phys. Lett., 2000, 76: 1776
63. Zhi C. Y., Bai X. D., and Wang E. G, Appl. Phys. Lett., 2002, 81: 1690
64. Fransen M., PhD Thesis, Technical University Delft (1999)
65. Bonard J. M., Dean K. A., Coll B. F., and Kilinke C., Phys. Rev. Lett., 2002, 89: 197602
66. Xu N. S., Chen Y., Deng S. Z., Chen J., Ma J. C., and Wang N. G., J. Phys. D, 2001, 34: 1579
67. Iijima S. and Ichihashi T., Nature, 1993, 363: 603
68. Bethune D. S., Kiang C. H., de Vries M. S., Gorman G., Savoy R., Vasquez J. and Beyers R., Nature, 1993, 363: 605
69. Dresselhaus M. S., Dresselhaus G., and Eklund P. C., Carbon, 1995, 33: 883
70. Mintmire J. W., Dunlap B. I., and White C. T., Phys. Rev. Lett., 1992, 68: 631
71. Wallace P. R., Phys. Rev., 1947, 71: 622
72. Saito R., Dresselhaus G., and Dresselhaus M. S., J. Appl. Phys., 1993, 73: 494
73. Charlier J.-C. and J.-P. Michenaud, Phys. Rev. Lett., 1993, 70: 1858
74. Lambin P., Philippe L., Charlier J.-C. and Michenaud J.-P., Comp. Mat. Sci. 1994, 2: 350
75. Ebbesen T. W., Lezec H. J., Hiura H., Bennett J. W., Ghaemi H. F. and Thio T., Nature, 1996, 382: 54
76. Frank S., Poncharal P., Wang Z. L. and de Heer W. A., Science, 1998, 280: 1744
77. Gao R., Pan Z. W. and Wang Z. L., Appl. Phys. Lett., 2001,78: 1757
78. Zhao J. J., Han J. and Lu J. P., Phys. Rev. B, 2002, 65: 193401
79. Ramprasad R., von Allmen P. and Fonseca L. R. C., Phys. Rev. B, 1999, 60: 6023
80. Forbes R. G., Surf. Interface Anal., 2004, 36: 395
81. Forbes R. G., J. Vac. Sci. Technol. B, 1999, 17: 526
82. Edgcombe C. J., Phys Rev B, 2005, 72: 045420
83. Han S. and Ihm J., Phys. Rev. B, 2000, 61: 9986
84. Jeong T., Appl. Phys. Lett., 2005, 87: 063112
85. Mayer A. and Lambin Ph., Carbon, 2002, 40: 429－436
86. Mayer A., Miskovsky N. M. and Cutler P. H., Ultramicroscopy, 2002, 92: 215－220
87. Forbes R., Edgcombe C. J., and Valdrè U., Ultramicroscopy, 2003, 95: 57－65
88. Kokkorakis G. C., Modinos A., and Xanthakis J. P., J. Appl. Phys., 2002, 91: 4580
89. Edgcombe C. J. and Valdrè U., Solid State Electron., 2001, 45: 857
90. Adessi Ch. and Devel M., Phys. Rev. B, 2002, 65: 075418
91. Bonard J.-M., Croci M., Arfaoui I., Noury O., Sarangi D., Chatelain A., Diamond and Related Materials, 2002, 11: 763－768
92. Smith R. C., et al, Appl. Phys. Lett., 2005, 87: 103112
93. Lee S. M., An K. H., Lee Y. H., Seifert G., and Frauenheim T., J. Am. Chem. Soc., 2001, 123: 5059－5063
94. Wadhawan A., Stallcup II R. E., Stephens II K. F., and Perez J. M., Appl. Phys. Lett., 2001, 79: 1867
95. Kim C. W., et al, Phys. Rev. B, 2003, 68:115403
96. Jhi S.-H., Louie S. G., and Cohen M. L., Phys. Rev. Lett., 2000, 85: 1710
97. Zhu X. Y., Lee S. M., Lee Y. H., and Frauenheim Th., Phys. Rev. Lett., 2000, 85: 2757
98. Park N., Han S., and Ihm J., Phys. Rev. B, 2001, 64: 125401
99. Sorescu D. C., Jordan K. D., and Avouris Ph., J. Phys. Chem. B, 2001, 105: 11227
100. Moon C.-Y., Kim Y. -S., Lee E.-C., Jin Y.-G., and Chang K. J., Phys. Rev. B, 2002, 65: 155401
101. Steckel J. A., Jordan K. D., and Avouris Ph., J. Phys. Chem. A, 2002, 106: 2572
102. Grujicic M., Cao G., and Gresten B., Appl. Surf. Science, 2003, 206: 167
103. Kim C. W., Choi Y. S., Lee S. M., Park J. T., Kim B. S., and Lee Y. H., J. Am. Chem. Soc., 2002, 124: 9906
104. Mayer A., Miskovsky N. M., Cutler P. H., and Lambin Ph., Phys. Rev. B, 2003, 68: 235401
105. Mayer A., Phys. Rev. B, 2005, 71: 235333
106. Cumings J., Zettl A., McCartney M. R., and Spence J. C. H., Phys. Rev. Lett., 2002, 88: 056804
107. Warshel A. and Levitt M., J. Mol. Biol. 1976, 103: 227
108. Yang W., Phys. Rev. Lett., 1991, 66: 1438
109. Tamura R. and Tsukada M., Phys. Rev. B, 1995, 52: 6015
110. Carroll D. L., Redlich P., Ajayan P. M., Charlier J. C., Blase X., de Vita A., and Car R., Phys. Rev. Lett., 1997, 78: 2811
111. Li Z. B. and Wang W. W., Chin. Phys. Lett., 2006, 23: 1618
112. Huang N.Y., et al, Phys. Rev. Lett., 2004, 93: 075501－1